IAC-19,C4,8-B4.5A,12

Development of N2O/HDPE Hybrid Rocket for Microsatellite Propulsion

Landon Kamps[a]*, Pau Molas-Roca[b], Erica Uchiyama[c], Tomohiro Takanashi[a], Harunori Nagata[a]

[a] *Faculty of Engineering, Hokkaido University, North 13 West 8, Sapporo, Hokkaido, Japan 060-8628,* kamps@eng.hokudai.ac.jp, takanashi@frontier.hokudai.ac.jp, nagata@eng.hokudai.ac.jp
[b] *Division of Space Technology, Luleå University of Technology, Rymdcampus 1, Kiruna, Sweden 981 92,* info@paumolasroca.com
[c] *Department of Mechanical and Space Engineering, Hokkaido University, North 13 West 8, Sapporo, Hokkaido, Japan 060-8628,* erika-u@eis.hokudai.ac.jp
* Corresponding Author

Abstract

This research compares the performance of three alternative hybrid rocket propulsion systems using liquid nitrous oxide and/or gas oxygen as the oxidizer for use as microsatellite thrusters. Internal ballistic performance predictions are based on recent experimental research and codified using the MATLAB App designer for open release. A self-pressurizing liquid nitrous oxide hybrid rocket thruster is shown to outperform a high-pressure gas oxygen hybrid rocket thruster in ΔV (1412 m/s versus 1326 m/s) and initial (wet) mass (95 kg versus 107 kg), even though time-averaged I_{sp} is smaller (300 s versus 317 s). This is because the gas oxygen system requires very high-pressure storage vessels (> 60 MPa) and a larger fuel grain which results in a heavier hybrid rocket motor. Nozzle erosion is included in this analysis, and shown to result in a positive feedback of oxidizer flow rate relative to fuel flow rate that prevents I_{sp} from decreasing in the liquid nitrous oxide thruster. The high-performing liquid nitrous oxide hybrid rocket thruster is produced in CAD, and shown to have adequate space for mounting all necessary sub-systems and payload modules, with room for future adjustments as necessary.
Keywords: Hybrid Rocket, Microsatellite, Apogee Kick, Internal Ballistics

Nomenclature

d	=	diameter, m
D	=	(mass) diffusivity, m^2/s
G_{ox}	=	(fuel) port mass flux, kg/m^2-s
I_{sp}	=	specific impulse, s
O/F	=	oxidizer-to-fuel-mass mixture ratio
P	=	pressure, Pa
$\dot{r}$	=	(fuel or nozzle) regression rate, m/s
Re	=	Reynold's number
Sc	=	Schmidt number of CO
T	=	temperature, K
ΔV	=	change in velocity, "delta V", m/s
Φ	=	equivalence ratio
ρ	=	density, kg/m^3

Subscripts

n	=	nozzle
w	=	nozzle wall

Acronyms/Abbreviations

CAD	=	Computer-Aided Design/Draft
CEA	=	(NASA) Chemical Equilibrium with Applications
GFRP	=	Glass Fiber-Reinforced Plastic
GTO	=	Geostationary Transfer Orbit
HDPE	=	High-Density Polyethylene
ISAS	=	Institute of Space and Astronautical Science (Japan)
JAXA	=	Japan Aerospace Exploration Agency
PMMA	=	Polymethyl Methacrylate
RCS	=	Reaction Control System
SHARE	=	Scalable Hybrid Apogee kick Rocket motor for space Exploration

1. Introduction

Of the 13 Japanese H2A-series rocket launches to Geostationary Transfer Orbit (GTO) or beyond since 2001, only three deployed payloads on missions to deep space: *Kaguya, Akatsuki and Hayabusa 2* [1]. The 10 launches which did not send payloads to deep space stand out as missed opportunities of the science and engineering community, especially of Japan and its partners. The H2A-series rockets have a piggyback capability for satellites sized roughly 600-800 mm in the outermost dimensions, which includes the category of microsatellites [2]. Thus, a microsatellite capable of producing its own thrust could deploy from GTO to deep space by piggybacking on the H2A or a similar rocket. The minimum change in velocity, i.e. ΔV, required to maneuver from GTO to Earth escape is roughly 700 m/s, however a change in velocity of 1000 m/s or more would greatly increase the possibility of conducting deep space science missions. For example, the delivery window for a microsatellite maneuvering from GTO to a Lunar orbit is roughly 1 day/year for a

ΔV of 700 m/s, but over 100 days a year for a ΔV of 1000 m/s.

Hybrid rockets are a promising alternative propulsion system category for satellites which piggyback to space, for their low/non-toxicity, non-explosiveness, robustness against temperature changes, storability, stop/restart ability and relatively high thrust [3,4]. Moreover, with few exceptions, hybrid rockets are easier to develop at academic, international and civilian research institutions than most chemical propulsion systems – liquid bi-propellant, solid, and liquid monopropellant systems included – for the wide-spread commercial availability of propellants, and the relative ease of handling and manufacturing of materials that make up a typical hybrid rocket.

1.1 Hybrid Rockets as Satellite Thrusters

Chandler et al. first reported on the feasibility of using hybrid rockets as space thrusters with the vision of using a hybrid rockets in place of liquid rockets for Mars orbital insertion missions [5]. They confirm that, "a hybrid system…can accomplish a Mars orbit insertion," which was stated in the context of four previously successful missions using liquid rocket engines – with ΔV ranging from 900-1600 m/s, initial masses of 700-2200 kg, and propellant mass fractions ranging from 20-55%. Chandler et al.'s design was based on the use of the liquid oxidizer MON3, which is predominately composed of nitrogen tetroxide (N_2O_4), however hydrogen peroxide (H_2O_2) and Nytrox, which is a combination of nitrous oxide (N_2O) and oxygen (O_2), were also mentioned as alternative oxidizers. They discounted H_2O_2 mainly for concerns regarding its decomposition over time, whereas Nytrox and its main constituent N_2O seem to have simply been overlooked.

More recently Jens et al. have reported on the development of a CubeSat-based hybrid rocket thruster for accelerating CubeSat-sized payloads to deep space from Earth orbit [6,7]. The latest version of their design known to the authors is a 12U-sized hybrid rocket thruster producing a ΔV of 800 m/s with an initial wet mass of 25 kg, although the payload mass allocation is not discussed in detail. Jens et al.'s design is based on the use of gaseous O_2 as the oxidizer, which will be stored at pressures above 60 MPa, and regulated before injection into the hybrid rocket motor. Jens et al. discounted N_2O as a candidate oxidizer citing its relatively low I_{sp} compared with O_2, 300 s versus 340 s, relatively low density compared with MON3 or H_2O_2, 800 kg/m^3 versus 1400 kg/m^3, and lack of space heritage [8].

1.3 N_2O/HDPE Hybrid Thruster Development

While discounted from Chandler et al. and Jens et al.s' development projects, liquid N_2O is being successfully employed in other major hybrid rockets operations. For example, at the beginning of this year (February 2019) Beth Moses became the first passenger astronaut in history, riding in the Virgin Galactic Unity spaceplane powered by an N_2O-based hybrid rocket motor [9]. Moreover, Yen-Sen Chen reported this summer (August 2019) plans for the launch of the first Hapith-V rocket, a three-stage-to-orbit hybrid rocket using N_2O as the main oxidizer for all three stages [10,11]. Both examples take advantage of the self-pressurizing ability of N_2O for the supply of oxidizer to the motor, and benefit from the storability of N_2O up to launch.

The authors saw liquid N_2O as an oxidizer worth considering for applications as satellite thrusters, and in FY2017 entered into a four-year collaborative research agreement with JAXA ISAS to investigate the potential of a N_2O-based hybrid rocket thruster, and develop a flight model for future piggyback missions to space [12].

Due to the general lack of open source information on the performance characteristics and internal ballistics of N_2O hybrid rockets using thermoplastic fuels, particularly HDPE, the first two years of this collaboration were spent conducting experimental firing tests on a sub-scale N_2O/HDPE hybrid rocket motor. In fact, the collection and analysis of ballistic data itself became a research topic, due to the complex interdependencies between measurable properties of combustion pressure, oxidizer mass flow rate and temperature, and difficult to measure properties of fuel mass flow rate, combustion efficiency and nozzle throat erosion. Kamps et al. first developed an innovative ballistic reconstruction technique and test procedure to measure the histories of fuel mass flow rate, nozzle throat diameter and combustion efficiency in [13]. This method was then used to investigate combustion efficiency by Kageyama et al. [14], graphite nozzle erosion by Kamps et al. [15], and fuel regression rate by Ito et al. [16]. During this time a performance prediction algorithm and computer program was developed and first used to investigate the trade-offs of pre-existing hybrid rocket alternatives for use as CubeSat thrusters [17]. This report concluded that for satellites larger than 12U, self-pressurizing liquid N_2O/HDPE hybrid rockets are most likely to outperform the alternatives due to savings in structural mass.

1.4 Microsatellite-based N_2O/HDPE Thruster

This study aims to predict the ΔV capability of N_2O-based hybrid rocket thrusters within the constraints of a microsatellite-size envelope, and compare the results to that when using a high-pressure gas O_2-based hybrid rocket thruster. Although the current status of this project is far from an operational flight model, the predictions made at this stage of development will help elucidate many of the knowledge gaps that currently exist regarding hybrid rocket thrusters in general.

Mainly, how much ΔV capability is lost due to plumbing mass for the oxidizer supply system? Can the motor fit within a conventional envelope shape? And how negative of an impact will nozzle erosion have on ΔV capability?

To complete these objectives in a coherent way, a summary of pertinent and recent experimental findings regarding N_2O/HDPE hybrid rocket ballistic performance will be reported first, followed by an overview of a computer program/algorithm that was created to deal with the large differences between oxidizer supply systems using liquid N_2O and gas O_2 and, as well as their varying internal ballistic performance dependencies. In fact, another major contribution of this work will be the introduction of an open-source and user-friendly MATLAB application for the design of hybrid rocket satellite thrusters, which is programmed to be adaptable to design constraints outside the purview of the current analysis.

2. Summary of Pertinent Experimental Research

Over the past two years dozens of static firing tests have been conducted by the authors of this paper and their colleagues to develop empirical formulations for key internal ballistic performance predictions using a sub-scale N_2O/HDPE motor and test apparatus. Much of this work has been reported on in open literature in preparation for the current study. It is the aim of this section to briefly introduce each subtopic along with the related publications, and summarize the relevant findings in the context of the development of a N_2O/HDPE microsatellite thruster. The topics discussed in this section include: combustion instability suppression, fuel regression rate prediction, nozzle throat erosion rate prediction, increasing combustion efficiency, and ignition criteria.

2.1 Similarities Between Experiments

A general depiction of the test motor is shown in Fig. 1. Essentially all basic research was conducted on some version of this test motor. The HDPE fuel material was supplied by Takada Chemical Industries Ltd, the graphite nozzles material (G347) was supplied by Tokai Carbon Ltd., and fuel was encased in glass-fibre reinforced plastic (GFRP) produced by Three Hope Ltd.

Lego-like fuel blocks were manufactured in bulk by the Hokkaido University Engineering Workshop technicians, and assembled to form the desired chamber/port design according the test being conducted. The motor was roughly 200 mm in length and 50 mm in diameter, which is half the size of the motor that can be expected for future use based on the analysis in Section 4. Results. All tests were conducted such that N_2O was supplied to the injector in the liquid phase.

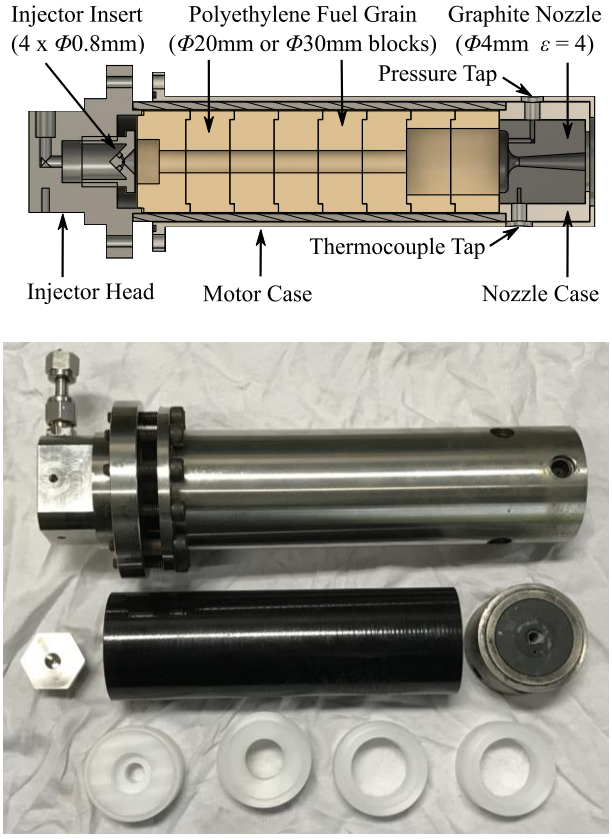

Fig. 1. Sub-scale N_2O/HDPE Test Motor

2.2 Combustion Instability Suppression

One of the first issues encountered when conducting experiments was large oscillations in chamber pressure during firing. This is evident in a plot of the chamber pressure history of an early experiment (see Fig. 2 upper). A straight injector with a single 0.8 mm diameter orifice restriction was initially used to cause a pressure drop that would vaporize the liquid N_2O being supplied to the motor with the intention of causing a choking effect that would supress pressure feedback within the flow system. However, this vaporization process had the opposite effect, resulting in acoustic feedback that caused dangerously large pressure oscillations of ±100% the nominal chamber pressure. Fortunately, this issue was easily overcome by implementing an impinging-jet of 4 x 0.8 mm holes at 45° (see Fig. 2 lower) which is not so restricting that the downstream pressure does not fall below the vapor pressure of N_2O. With the new injector, pressure oscillations were less than ±3% of the nominal value.

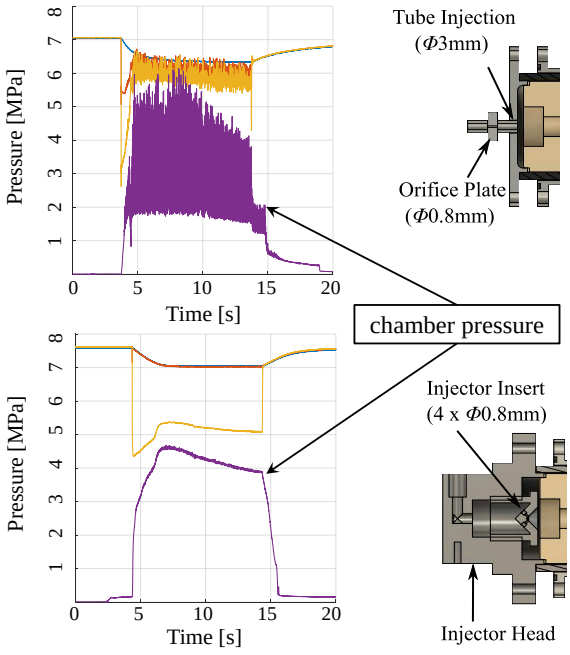

Fig. 2. Suppression of pressure oscillations

2.3 Fuel Regression Rate Formulation

Ito et al. [16] reported on the findings of fuel regression rate correlations based on experiments conducted in preparation for this study. They concluded that fuel regression rate is predominately a function of oxidizer mass flux, according to Marxman's diffusion limited model [1], but in fuel rich conditions a pressure dependency emerges. This can be explained by the increased presence of soot in fuel rich conditions, which acts as a black body emitting radiative heat form the flame to the fuel surface. Although four formulations were shown to adequately capture this behaviour, the one selected for this study is Eq. (1):

$$\dot{r} = (0.05)P^{0.15\Phi^4 \exp(-\Phi)}G_{ox}^{0.47} \qquad (1)$$

In this equation, the pressure exponent tends to zero when equivalence ratio drops below unity, and increases to a maximum value of around 0.7 for an equivalence ratio Φ around 4. Note that equivalence ratios above 3 are not expected to occur in actual firing conditions, thus for practical purposes, the pressure exponent can be thought to reach a maximum value of around 0.5 in very fuel rich conditions. The exponent of oxidizer port mass flux term, G_{ox}, is 0.47, close to the theoretical value for diffusion-limited combustion within a laminar boundary layer. This exponent likely results from the fact that the fuel is not long enough for a fully developed turbulent boundary layer to develop. In the full-scale microsatellite thruster, which is twice as long, this exponent may increase to a value closer to 0.8 according to Marxman's theory for turbulent boundary layer combustion.

Figure 3 plots a re-representation of the results of Ito et al., so that the general trend can be compared with that of previous research by Doran et al. [18] and Moon et al. [19] which used time-averages for regression rate, and did not cover a large range of chamber pressures or equivalence ratio. One conclusion that can be drawn from Fig. 3 is that even though the phenomena of fuel regression are better represented by Eq. (1) than time-averaged correlations of previous research, the overall discrepancy between models is less than 25% for a wide range of time-averaged port mass fluxes (70-170 kg/m^2-s), as well as equivalence ratio and chamber pressure.

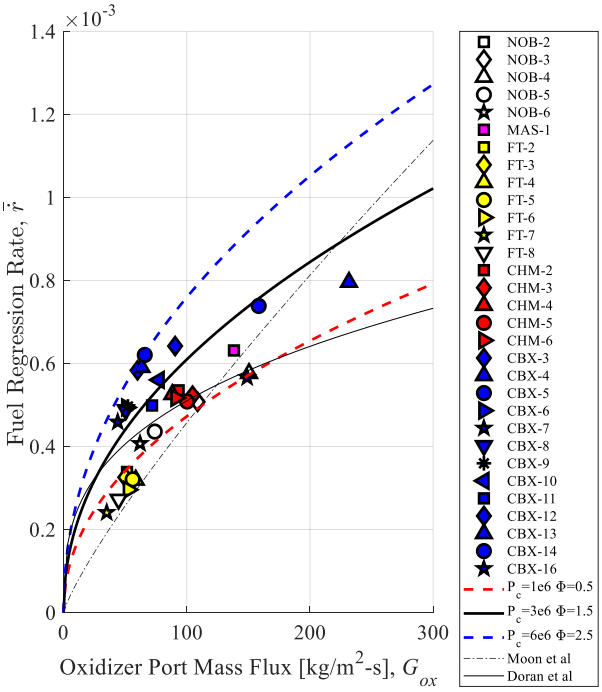

Fig. 3. Time-averaged regression rate representation of Ito et al.'s experiments for comparison with previous research

2.3 Graphite Nozzle Erosion

Kamps et al. report the results of graphite nozzle erosion rate correlations in [15]. This report is part of a doctoral thesis that investigates nozzle erosion in hybrid rockets using both N_2O and O_2 as oxidizers at various scales [20]. The model for N_2O is Eq. (2):

$$\begin{aligned} &\rho_n \dot{r} = \beta * \Pi * \mathrm{K} \\ &\rightarrow \beta = 4.46\Phi^{-2.09}\exp\left(-3.77\Phi\right) \\ &\rightarrow \Pi = T_w^{-0.07}\exp\left(-2996/T_w\right)P^{0.15} \\ &\rightarrow \mathrm{K} = \left(\rho D\right)\Big/\left(43.3d\,\mathrm{Re}^{-0.83}\,\mathrm{Sc}^{-0.44}\right) \end{aligned} \qquad (2)$$

Here the three Greek alphabet terms on the right-hand side of the equation represent three separate dependencies of the thermochemical erosion of graphite. The first term, β, represents the dependency of oxidizing species concentration and combustion gas temperature on equivalence ratio. The second term, Π, represents the activation energy/reactivity of the graphite nozzle. This term is highly dependent on the nozzle wall temperature exposed to the combustion gas. The third term, K, represents the diffusion-limiting effect of the concentration boundary layer. The diffusion term ρD on the right-hand side of the K-term equation is the product of density and mass diffusivity of nozzle erosion product gas CO calculated at the nozzle wall temperature.

2.4 Combustion Efficiency

Kageyama et al. [14] report on findings of the effect of the aft chamber geometry on combustion efficiency. As is shown in Fig. 1, the fuel blocks – or in some cases graphite blocks – located just upstream of the nozzle are made to have a more voluminous port than the mid-section of the fuel. This is a common geometry for hybrid rockets, and is generally recognized to improve mixing. The characteristic exhaust length term, L^*, can be applied to this aft chamber as a way of representing the residence/mixing time of combustion gas. Kageyama et al. show that although increasing L^* improves the combustion efficiency, having a sudden change in port geometry entering and exiting the aft chamber is possibly equally as important as the magnitude of L^*. Both Kageyama et al. [14] and Kamps et al. [13] report cases where combustion efficiency reached 95% after a short transient during start-up and remained relatively constant until motor shutdown.

2.5 Ignition Criteria

Several reusable ignitors have been developed by other hybrid rocket research groups, and shown to be operational even in deep vacuum. Whitmore et al. [21,22] demonstrated successful back-to-back ignitions using arc-ignitor system in space, and a collaboration between Dyrda et al. [23] and Jens et al. [7] resulted in dozens of successful back-to-back ignitions of a O_2/PMMA hybrid rocket motor in a vacuum chamber, using both a diode laser ignitor as well as a gas O_2/methane ignitor. Faenza et al. [24] use a catalytic ignition system on the Nucleus hybrid rocket propulsion system, which can, in theory, be modified and applied to the motor of this study since N_2O is known to be a thermally energetic monopropellant when heated and passed through a catalyst bed [25,26].

The ignition method used in all experiments for this study has been the heating of a 20 mm length of nichrome wire attached to the first fuel block with 1 g of epoxy until red hot using a DC voltage source, and running oxidizer into the motor. Although this has the main drawback of being one-time-use, it is surprisingly effective. The multitude of differing ignition systems essentially speaks to one key attribute of hybrid rocket ignition. Since the oxidizer flow rate can be controlled by actuating a valve, ignition rarely, if ever, takes place in a complete vacuum. The oxidizer passing into the combustion chamber has some absolute pressure, which means combustion can be initiated so long as the fuel is heated to its pyrolysis temperature and the oxidizer velocity is not so large that blow off occurs.

Nonetheless, the minimum pressure or maximum gas velocity that should be avoided to ensure combustion have not been reported in previous studies. For this reason, the authors of this paper conducted several experiments under low-pressure conditions to further investigate the risk of blow off. The results of these ignition tests are shown in Fig. 4. Although the data are sparse, it can be said that the ignition of N_2O/HDPE under heating by nichrome wire was unsuccessful when absolute pressure was less than 0.06 MPa (or 0.6 atm). This is best demonstrated by comparison of the data at oxidizer velocities of around 15 m/s. There are not enough data to comment in detail about the influence of oxidizer velocity, however, the proximity of the x-coordinate of data compared with the y-coordinate to the left and right of the undetermined case (black triangle in Fig. 4) suggests that pressure is the determining factor of N_2O ignition.

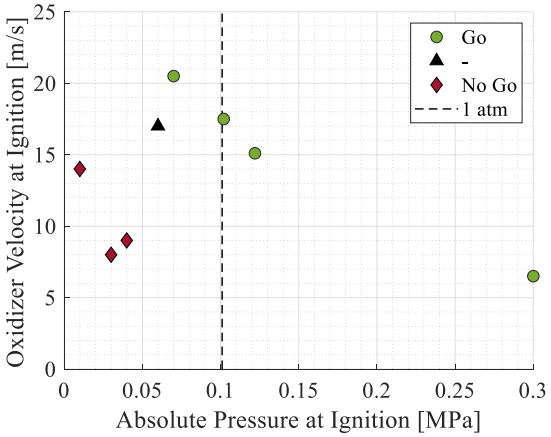

Fig. 4. Conditions at the time of ignition of N_2O/HDPE

3. Design Algorithm & MATLAB Application Suite

The design algorithm used for this study (see Fig. 5) is a slightly modified version of that presented by Kamps et al. in [17]. The governing equations remain the same, with chamber pressure and combustion gas mixture calculations made using NASA CEA [27], thrust calculated as a frozen flow expansion in the nozzle, and pressure vessel mass modelled after actual values from industry catalogs [28,29]. However, this

algorithm has since then been updated and codified, using MATLAB App Designer with the intent of releasing it as an open source software. The program has not been released yet, so interested parties should contact the corresponding author directly for access to the code until it is made available online or through the MATLAB app exchange. For details of the governing equations, the reader should check [17], or consult the user manual upon public release version of the code. A brief description of key assumptions and the calculation strategy will be discussed in this section.

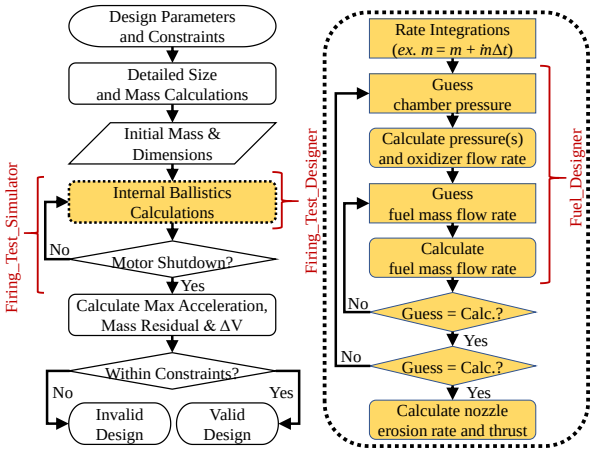

Fig. 5. Calculation flowchart of thruster performance. *Separate MATLAB Apps available for processes in red*

3.1 Calculation Strategy

The calculation of hybrid rocket motor performance is inherently implicit due to the numerous non-linear dependencies between ballistic terms of combustion pressure, equivalence ratio, mass flow rate, and fuel and nozzle regression rates. However, treating the sizing and performance prediction of the entire microsatellite thruster as an implicit calculation results in problems of divergence of solutions and/or impossible solutions – such as negative mass or positive pressure "drops" in the flow direction etc. To overcome this issue, the internal ballistic calculations at any given time are solved for implicitly using the bisection method, and these results are integrated in time to determine the satellite performance. This process continues in time until one of the propellants runs below the minimum residual designated by the user, or the time reaches the maximum time designated by the user. Then a filter is applied to discount any solutions that do not meet the maximum acceleration or maximum propellant residual constraints set by the user.

3.2 Subordinate Apps as Design and Experiment Tools

The main app for designing a satellite-based hybrid rocket thruster is titled, "SHARE_Designer," short for "Scalable Hybrid Apogee kick Rocket motor for space Exploration," however three additional MATLAB Apps were created (see Appendix A), the purviews of which are shown in Fig. 5 using dark red brackets. Since the governing equations for designing and predicting the performance of the microsatellite thruster are also the same equations required for planning and conducting experimental firing tests, these three additional applications were easy to create as subsidiaries of calculations already taking place.

For example, the mass flow rate of fuel is solved implicitly using the bisection method. The "Fuel_Designer" app was created to allow the user to investigate the solution space of fuel design-related parameters without running the SHARE_Designer. Fig. 6 is a plot produced using this app for an N_2O/HDPE motor with a single port fuel grain that is 100 mm in diameter and 300 mm in length with a fuel fill factor of 95% (i.e. port diameter of 22 mm). Similar analysis can be done using the "Firing_Test_Designer" for selecting the appropriate flow system components and measurement tools, i.e. injector size, appropriately rated load cell etc.; and the "Firing_Test_Simulator" for predicting the progression of internal ballistics behavior in time, such as the increase in nozzle throat diameter or burn through of fuel etc.

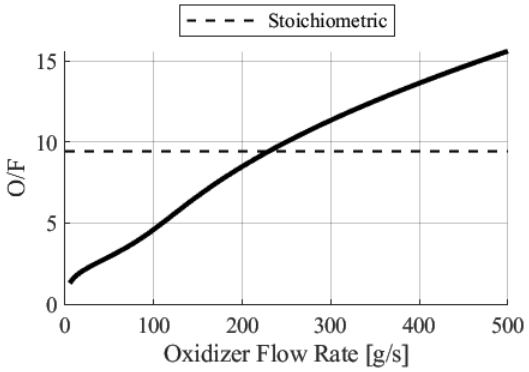

Fig. 6. Example plot of mixture ratio (O/F) solution space produced using the Fuel_Designer app. *N_2O/HDPE, (single) 22 mm port fuel 300 mm in length*

4. Hybrid Rocket Thruster Designs & Comparisons

In this section the ΔV capability of N_2O-based hybrid rocket thrusters will be predicted and compared with the results to that when using a high-pressure gas O_2-based hybrid rocket thruster. These results were produced using the MATLAB suite described in Section 3, based on the experimental results summarized in Section 2.

4.1 Performance Designations and Constraints

The SHARE_Designer App has been set up so that the user can manipulate numerous parameters to improve the design at hand. However, due to the large number of parameters, it is necessary to list and explain

the most pertinent ones here (see Table 1). All comparisons will be based on the same basic envelope of a 550 mm cube, which was found to be small enough and light enough to piggyback on the H2A-series rockets, with some freedom for increasing either the outer dimensions or instrument mass as necessary.

Table 1. Pertinent designations and constraints

System designations:	Value	Units
envelope width & height	550	mm
height factor (vessels & motor)	80	%
diameter factor (vessels & motor)	80	%
safety factor (vessels)	1.5	
thickness factor (case & shield)	3	%
nozzle height ratio	12	
nozzle expansion ratio	100	%
flow restriction diameters (1/2")	6	mm
temperature (gas and liquid)	288	K
efficiency (combustion & thrust)	95	%
Shutdown Criteria:		
maximum burn time	600	s
minimum oxidizer mass residual	10	%
minimum fuel residual	5	%
Performance Constraints		
maximum acceleration	3	G
maximum fuel mass residual	100	%
maximum oxidizer mass residual	100	%
Fixed Mass Estimates:		
ignitor	1	kg
RCS	4	kg
valves (and related plumbing)	5	kg
communications bus	5	kg
structure	10	kg

The hybrid rocket motor and pressure vessels are set to 80% of the envelop height (i.e. 440 mm), and the thickness of the motor case and shield are set to 3% of their respective diameters – these values vary during parametric analysis. The nozzle is assumed to be bell-shaped for performance purposes, where the distance from the throat to the exit is 12 times the throat diameter and the expansion ratio is 100. However, the nozzle skirt is assumed to be a conical cone of similar dimensions for the mass calculation. The plumbing is assumed to be 1/2" tubing through out (inner diameter of around 6 mm). Combustion and thrust efficiencies are both assumed to be 95%, resulting in an effective efficiency of roughly 90%. The internal ballistic calculations end – i.e. the motor is "shutdown" – if the burn time exceeds 600 s, the oxidizer mass residual falls below 10%, or the fuel mass residual falls below 5%. Results of tests which have a maximum acceleration greater than 3 G (i.e. 29 m/s^2) are not considered as "valid" alternatives. The mass estimate for the structure is 10 kg, which is based on the detailed CAD design of Section 4.3. The ignitor, RCS, plumbing/valves and communications bus are items which have not been fixed and so the mass estimates are being made for safe measure, but do not reflect the actual sub-systems that will be used in future development.

4.2 Design Comparison

Three cases will be compared in this section: *Case A*, *Case B*, and *Case C*. Case A is the baseline self-pressurized liquid N_2O/HDPE thruster, Case B is the baseline gas O_2/HDPE thruster, and Case C is a pressure-fed liquid N_2O/HDPE thruster where gas oxygen is used to keep the N_2O pressurized above the vapor pressure (> 4.5 MPa at 288 K) for the full duration of N_2O supply, after which the gas O_2 becomes the oxidizer and is supplied to the motor. The purpose of considering Case C is to plan accordingly for the possibility of achieving greater performance through the combination of gas O_2 and liquid N_2O motors, however the details of the plumbing required to realize this type of motor is outside the scope of the current analysis.

The results of Cases A-C are summarized in Table 2 for a fixed payload mass of 20 kg. A comparison of ΔV capabilities for payload masses ranging from 0 to 40 kg is shown in Fig. 7. Cutaway schematics obtained through the SHARE_Designer application are placed in Appendix B due to their size.

Case A, the baseline liquid N_2O/HDPE thruster, achieves the largest ΔV of 1412 m/s. This is true even though the time-averaged I_{sp} is less than that of Case B, 300 s versus 317 s. Furthermore, this superior ΔV (of Case A) is achieved with an initial mass 12 kg lighter than Case B, 95 kg versus 107 kg. A review of the pressure vessel, case, shield, and nozzle masses (bottom of Table 2) shows that the gas O_2/HDPE thruster of Case B results in a much larger motor mass, which is the consequence of having a larger diameter fuel grain. The motor is not designed in the same way as the pressure vessels, so the penalty of requiring a larger fuel grain is more severe than that of requiring larger pressure vessels. Furthermore, the mass of the oxidizer vessels is also larger in Case B than in Case A because the pressure vessels of Case B require burst pressures of 90 MPa (60 MPa x 1.5 safety factor). Case C has relatively low performance while requiring a more complicated flow system, so it should be avoided if possible. The reason Case C might be of interest in the future is for ease of throttling. So long as the gas O_2 remains above the N_2O vapor pressure (> 4.5 MPa), the liquid N_2O can be throttled over a wide range of flow rates and thrusts. Throttling in Case A is not an option because any pressure drop in the flow system will cause vaporization of N_2O. Throttling in Case B is possible,

however, since the gas O_2 is choked at the injector, the range of flowrates for throttle is significantly limited.

Table 2. Summary of hybrid rocket thruster comparison

Parameter		Unit	Test Case A (N_2O)	B (O_2)	C (Mix)
ΔV		m/s	1412	1326	752
total mass	initial	kg	95	107	82
	final		59	70	69
thrust	average	N	1206	378	1273
I_{sp}	average	s	300	317	291
time		s	88	303	43
O/F	initial		35/4	32/9	20/3
	final		3/0.3	3/1	1/1
fuel	height	mm	410	410	410
	diameter		122	193	97
injector	holes	#	8	5	8
	diameter	mm	1	1	1
throat	initial	mm	14	10	15
	final	mm	19	16	19
regulator	pressure	MPa		10	10
gas press.	initial	MPa	4.5*	60	60
	final	MPa		6	4
pressure vessel mass		kg	7	13	11
case/shield/noz. mass		kg	4	8	3

* vapor pressure at 288 K

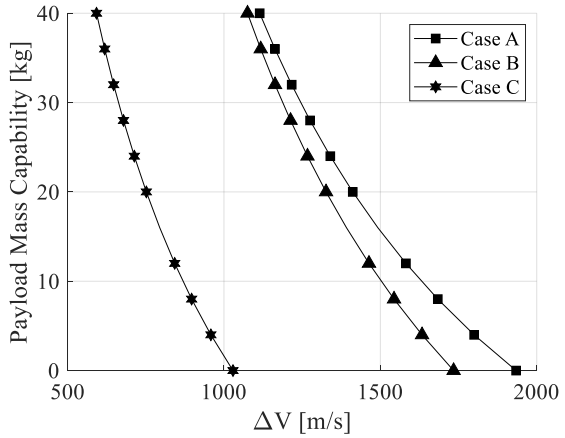

Fig. 7. Comparison of payload mass capabilities.

4.3 In-Depth Analysis of Self-Pressurized N_2O/HDPE Thruster (Case A)

The microsatellite-thruster system of Case A, the baseline self-pressurized liquid N_2O/HDPE thruster, was designed in CAD to confirm the estimated structural mass, visualize the vacant space available for mounting the payload, and prepare for development of the full-scale test motor and flight model [30]. A cutaway rendering of the design is shown in Fig. 7. It is clear from in inspection of Fig. 7 that due to a diameter factor of 80% (see Table 1) there is plenty of space between the vessels and motor, enough so even that a 6U payload (yellow box in Fig. 7) can fit between vessels – although the intent is to place the payload in the upper compartment with the valves and bus. At this stage in development the components, i.e. the vessels, electronics etc., have not been selected yet, so it is advantageous to have space available between components to allow for adjustments. However, it seems likely that the flight model version of this thruster may take on a smaller volume, which will translate to a smaller mass and thus higher ΔV.

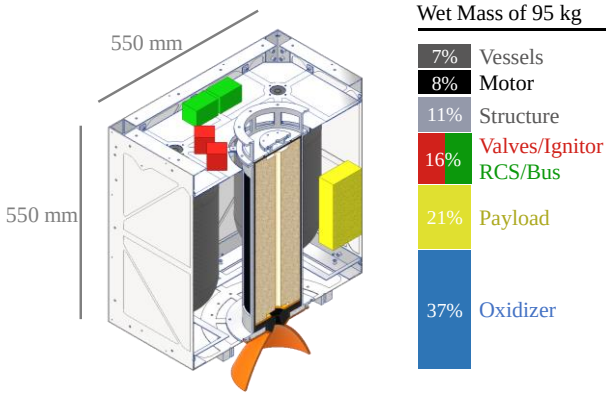

Fig. 8. Self-Pressurized liquid N_2O/HDPE microsatellite thruster CAD rendering and mass breakdown.

The time traces of internal ballistic predictions are shown in Figs. 9 thru 14. Based on the results of these figures, it is clear that nozzle throat erosion is a driving force in the outcome of performance. The nozzle throat increases in diameter by 71% (see Fig. 9), which is the leading cause of the drop in chamber pressure from 3 to 1.5 MPa (see Fig. 10). This drop in pressure causes the oxidizer mass flow rate to increase (see Fig. 11), which leads to an increase in thrust (see Fig. 12). Meanwhile, the port regression rate decreases with the increase in port diameter and decrease in chamber pressure (see Fig. 13). The decrease in port regression rate is less than the increase in the burning surface area is faster, and so the fuel mass flow rate increases in time (see Fig. 14).

Even though the throat diameter increase to nozzle erosion is significantly large, the I_{sp} is surprisingly constant in time (see Fig. 13). The decrease in I_{sp} due to the loss in expansion ratio appears to be made up for by a shift in mixture ratio towards the optimal value as the oxidizer flow rate increases relative to the fuel mass flow rate. This may not be the case when nozzle erosion rate is larger. The erosion rate predicted for this thruster is a mere 0.05 mm/s, which is low even for solid rocket motors.

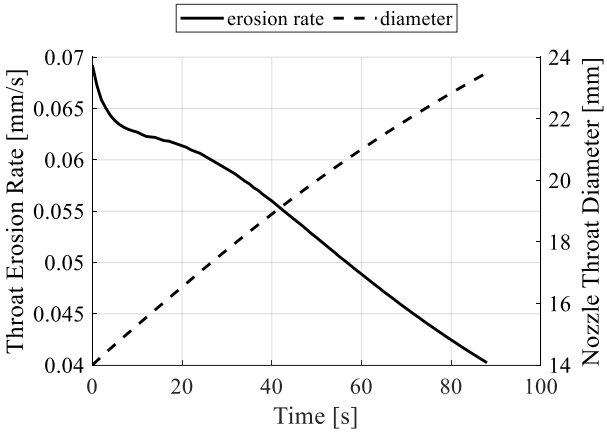

Fig. 9. Nozzle throat erosion rate decreases in time, but throat diameter increases by 71%.

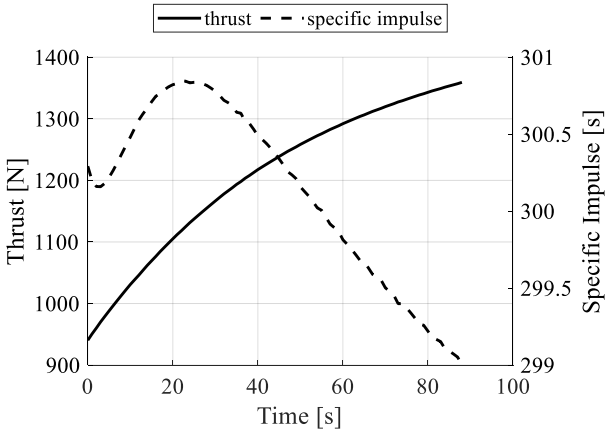

Fig. 12. Thrust increases and I_{sp} is relatively constant.

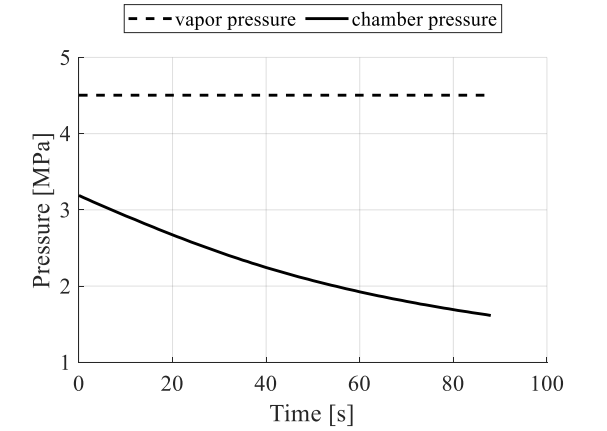

Fig. 10. Pressure drop due to nozzle throat erosion.

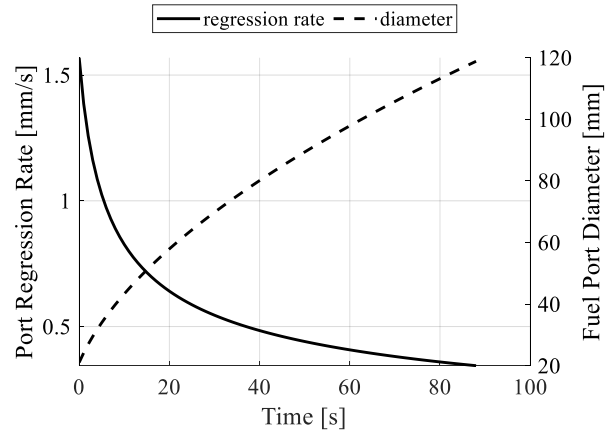

Fig. 13. Regression rate decreases with increasing port diameter and decreasing pressure due to throat erosion.

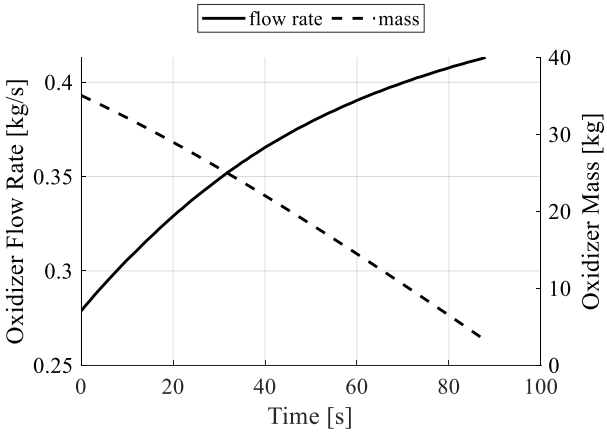

Fig. 11. Oxidizer mass flow rate increases due to nozzle throat erosion and the chamber pressure decrease.

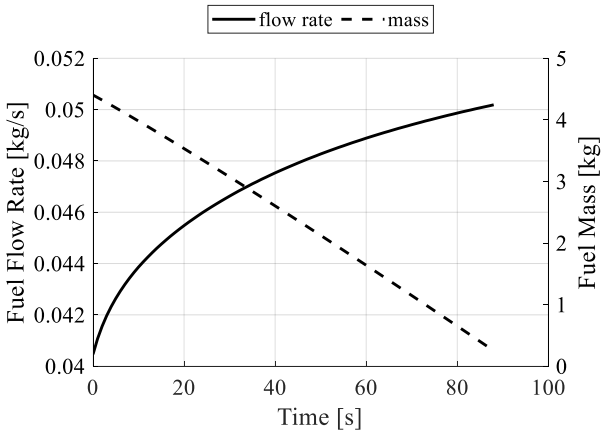

Fig. 14. Fuel mass flow rate decreases slightly.

5. Discussion and Plan for Future Work

The results of Case A analysis and design show a promising opportunity for conducting apogee kick missions and interplanetary orbital changes. However, these results have yet to be verified experimentally. The foundation of internal ballistic calculations are empirical formulations based on the results of sub-scale (1:2 Case A) and relatively short firing duration experiments (15 s or less). One example providing evidence that long-duration and large-scale firings of liquid self-pressurizing N_2O-based hybrids will not face insurmountable challenges are numerous successful suborbital space flights of Virgin Galactic Ltd. (see [9]). Nonetheless, the highest priority task for the next phase of development of the microsatellite thruster presented in this paper as Case A is the full-duration firing of a full-scale motor in a low-pressure environment. A full-scale experimental test motor and high-altitude simulation hybrid rocket chamber are already under construction at Uematsu Electric Co. Ltd., Akabira, Japan. A photograph of the chamber and CAD rendering of the internal configuration are shown in Fig. 15. Thrust will be measured in six degrees of freedom by suspending the motor from eight tension/compression load cells. All components have been assembled, and initial testing is schedule to begin in Winter of this year.

6. Conclusions

With the increasing readiness level of hybrid rocket motors and related technologies, there is a rich opportunity to lower the cost and increase the frequency of opportunities for missions to deep space using microsatellites. In Japan alone there are roughly 1-2 rocket launches to Geostationary Transfer Orbit every two years, which are within 700 m/s of travel to deep space and are equipped to carry multiple microsatellite payloads in piggyback configuration. More than one research group is aiming to fill this niche operating space using hybrid rockets, but the potential of using the self-pressurizing nitrous oxide has been largely overlooked. This study shows that the disadvantages of a nitrous oxide-based hybrid rocket thruster, mainly the relatively low density and specific impulse compared with other liquid oxidizers, are outweighed by the advantages of relatively low-pressure storage vessels and the alleviation of the requirement for pressure regulation and related plumbing. The results of computer simulations of internal ballistic performance and structural mass requirements based on two years of experimental research show that a self-pressurizing liquid nitrous oxide-based hybrid rocket microsatellite thruster outperforms a comparable high-pressure gas oxygen thruster in both mass and ΔV. A 550 mm cubic microsatellite equipped with a liquid nitrous oxide/high-density polyethylene hybrid rocket thruster with a ΔV capability of > 1400 m/s is predicted to have an initial wet mass of 95 kg when carrying a 20 kg payload. This accounts for a separate electronics bus of 10 kg and an RCS system of 4 kg.

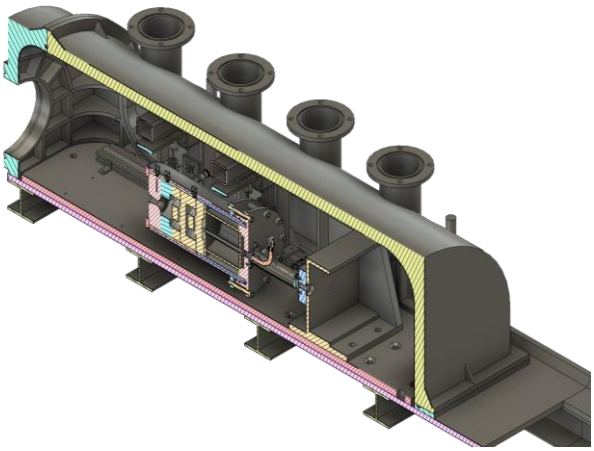

Fig. 15. High altitude simulation chamber under construction for full-scale hybrid rocket thruster testing.

Acknowledgements

The authors would like to recognize the contribution of Professor Kawakatsu and Assistant Professor Ozaki of JAXA ISAS for calculating the ΔV requirements for orbital transfer from GTO to Lunar orbit as mentioned in the introduction.

This research was supported financially by the Grant-in-Aid for Japan Society of Promotion of Science (JSPS) fellows 18J2087708, as well as by a matching fund program of Centers for Inter-University Collaboration from ISAS (Institute of Space and Astronautical Science), JAXA (Japan Aerospace Exploration Agency).

References

[1] About H-IIA Launch Vehicle; Launch Records, https://global.jaxa.jp/projects/rockets/h2a/, (accessed 7.10.19).

[2] H-IIA User's Manual, Ver. 4.0, February 2015, https://www.mhi.com/jp/products/pdf/manual.pdf, (accessed 15.03.19).

[3] D. Altman, A. Holzman, Overview and History of Hybrid Rocket Propulsion, in: M. J. Chiaverini, K.K. Kuo, Fundamentals of Hybrid Rocket Combustion and Propulsion, Progress in Aeronautics and Astronautics Vol. 218, AIAA Inc., Reston, 2007, pp. 1–33.

[4] S. Heister, E. Wernimont, Hydrogen Peroxide, Hydroxyl Ammonium Nitrate, and Other Storable Oxidizers, in: M.J. Chiaverini, K.K. Kuo, Fundamentals of Hybrid Rocket Combustion and Propulsion, Progress in Aeronautics and Astronautics Vol. 218, AIAA Inc., Reston, 2007, pp. 457–485.

[5] A.A. Chandler, B.J. Cantwell, G.S. Hubbard, Hybrid Propulsion for Solar System Exploration, AIAA Paper 2011-6103, 47th AIAA/ASME/SAE/ASEE Joint Propulsion Conference & Exhibit, San Diego, USA, 2011, 31 July – 3 August.

[6] E.T. Jens, A.C. Karp, J. Rabinovitch, B. Nakazono, A. Conte, D. Vaughan, Design of Interplanetary Hybrid CubeSat and SmallSat Propulsion Systems, AIAA Paper 2018-4668, 2018 Propulsion and Energy Forum, Cincinnati, USA, 2018, 9 – 11 July.

[7] E.T. Jens, A.C. Karp, K. Williams, B. Nakazono, J. Rabinovitch, Low Pressure Ignition Testing of a Hybrid SmallSat Motor, AIAA Paper 2019-4009, 2019 Propulsion and Energy Forum, Indianapolis, USA, 2019, 19 – 22 August.

[8] E.T. Jens, B.J. Cantwell, G.S. Hubbard, Hybrid Rocket Propulsion Systems for Outer Planet Exploration Missions, Acta Astronautica 128 (2016) 119–130.

[9] J. Fortin, Virgin Galactic Sends a Rocket Plane to Space Again, in Its Highest Flight Yet, 22 February 2019, https://www.nytimes.com/2019/02/22/science/virgin-galactic-space.html/, (accessed 07.10.19).

[10] Y.-S. Chen, Development of Hapith Small Launch Vehicle Based on Hybrid Rocket Propulsion, AIAA Paper 2019-3837, 2019 Propulsion and Energy Forum, Indianapolis, USA, 2019, 19 – 22 August.

[11] Hapith V, http://www.tispace.com/launch.html, (accessed 07.10.19).

[12] Matching Funds Program of Center for Inter-University Collaboration from ISAS, http://www.isas.jaxa.jp/researchers/partners/, (accessed 07.10.19).

[13] L. Kamps, K. Sakurai, Y. Saito, H. Nagata, Comprehensive Data Reduction for N_2O/HDPE Hybrid Rocket Motor Performance Evaluation, Aerospace 6 (2019) 45.

[14] L. Kageyama, L. Kamps, H. Nagata, Effect of Aft Chamber Volume on Hybrid Rocket Combustion Efficiency, AIAA Paper 2019-4334, 2019 Propulsion and Energy Forum, Indianapolis, USA, 2019, 19 – 22 August.

[15] L. Kamps, K. Sakurai, K. Ozawa, H. Nagata, Investigation of Graphite Nozzle Erosion in Hybrid Rockets Using N_2O/HDPE, AIAA Paper 2019-4264, 2019 Propulsion and Energy Forum, Indianapolis, USA, 2019, 19 – 22 August.

[16] S. Ito, L. Kamps, K. Sakurai, K. L. Kageyama, T. Okuda, H. Nagata, Fuel Regression Characteristics in Hybrid Rockets Using N_2O/HDPE, AIAA Paper 2019-4102, 2019 Propulsion and Energy Forum, Indianapolis, USA, 2019, 19 – 22 August.

[17] L. Kamps, Y. Saito, T. Viscor, T. Totani, H. Nagata, Feasibility Study on the Application of Hybrid Rockets as Onboard CubeSat Thrusters, 2019-a-20, 32nd International Symposium on Space Technology and Sciences, Fukui, Japan, 2019, 15 – 21 June.

[18] E. Doran, J. Dyer, K. Lohner, Z. Dunn, B. Cantwell, G. Zilliac, AIAA Paper 2007-5352, Nitrous Oxide Hybrid Rocket Motor Fuel Regression Rate Characterization, 43rd AIAA/ASME/SAE/ASEE Joint Propulsion Conference & Exhibit, Cincinnati, USA, 2007, 8 – 11 July.

[19] H. Moon, S. Han, Y. You, M. Kwon, Hybrid Rocket Underwater Propulsion: A Preliminary Assessment, Aerospace 6 (2019) 28.

[20] L. Kamps, Mechanisms of Graphite Nozzle Erosion in Hybrid Rockets, Ph.D. Dissertation, Hokkaido University, Japan, 2019.

[21] S.A. Whitmore, M.A. Bulcher, Vacuum Test of a Novel Green-Propellant Thruster for Small Spacecraft, AIAA Paper 2017-5044, 53rd AIAA/SAE/ASEE Joint Propulsion Conference, Atlanta, USA, 2017, 10 – 12 July.

[22] S.A. Whitmore, I.W. Armstrong, M. C. Heiner, C. J. Martinez, High-Performing Hydrogen Peroxide Hybrid Rocket with 3-D Printed and Extruded ABS Fuel, AIAA Paper 2018-4443, 2018 Propulsion and Energy Forum, Cincinnati, USA, 2018, 9 – 11 July.

[23] D.M. Dyrda, F.S. Mechentel, B.J. Cantwell, A.C. Karp, J. Rabinovitch, E.T. Jens, Diode Laser Ignition Testing for PMMA/GOX Hybrid Motors,

AIAA Paper 2019-4095, 2019 Propulsion and Energy Forum, Indianapolis, USA, 2019, 19 – 22 August.

[24] M.G. Faenza, A.J. Boiron, B. Haemmerli, O. Verberne, Development of the Nucleus Hybrid Propulsion System: Enabling a Successful Flight Demonstration, AIAA Paper 2019-3839, 2019 Propulsion and Energy Forum, Indianapolis, USA, 2019, 19 – 22 August.

[25] K. Lohner, J. Dyer, E. Doran, Z. Dunn, B. Krieger, V. Decker, E. Wooley, A. Sadhwani, B. Cantwell, T. Kenny, Design and Development of a Sub-Scale Nitrous Oxide Monopropellant Gas Generator, AIAA Paper 2007-5463, 43rd AIAA/ASME/SAE/ASEE Joint Propulsion Conference & Exhibit, Cincinnati, USA, 2007, 8 – 11 July.

[26] L. Hennemann, J.C. Andrade, F.S. Costa, Experimental Investigation of a Monopropellant Thruster Using Nitrous Oxide, J. Aerosp. Technol. Manag. 6 (2014) 363-372.

[27] S. Gordon, B. McBride, "Computer Program for Calculation of Complex Chemical Equilibrium Compositions and Applications, NASA RP-1311, 1994.

[28] General Dynamics, Ordinance and Tactical Systems, Composite Pressure Vessels, 2014, https://www.gd-ots.com, (accessed 19.10.18).

[29] Cobham Mission Systems, Composite Pressure Vessel Product List, 2016, https://www.cobham.com, (accessed 19.10.18).

[30] P. Molas-Roca, Design of a Scalable Hybrid Rocket Motor for Space Propulsion Applications, IAC-19-E2.2.1, 70th International Astronautical Congress, Washington D.C., USA, 2019, 21 – 25 October.

Appendix A (MATLAB App Suite Prototype)

→ SHARE_Designer: for the design of a satellite-based hybrid rocket thruster

→ Firing_Test_Simulator (app) : for the prediction of internal ballistic performance of a single motor

→ Firing_Test_Designer (app) : for the design of static firing test initial conditions (not shown below)

→ Fuel_Designer (app) : for the design of the appropriate fuel for static firing tests.

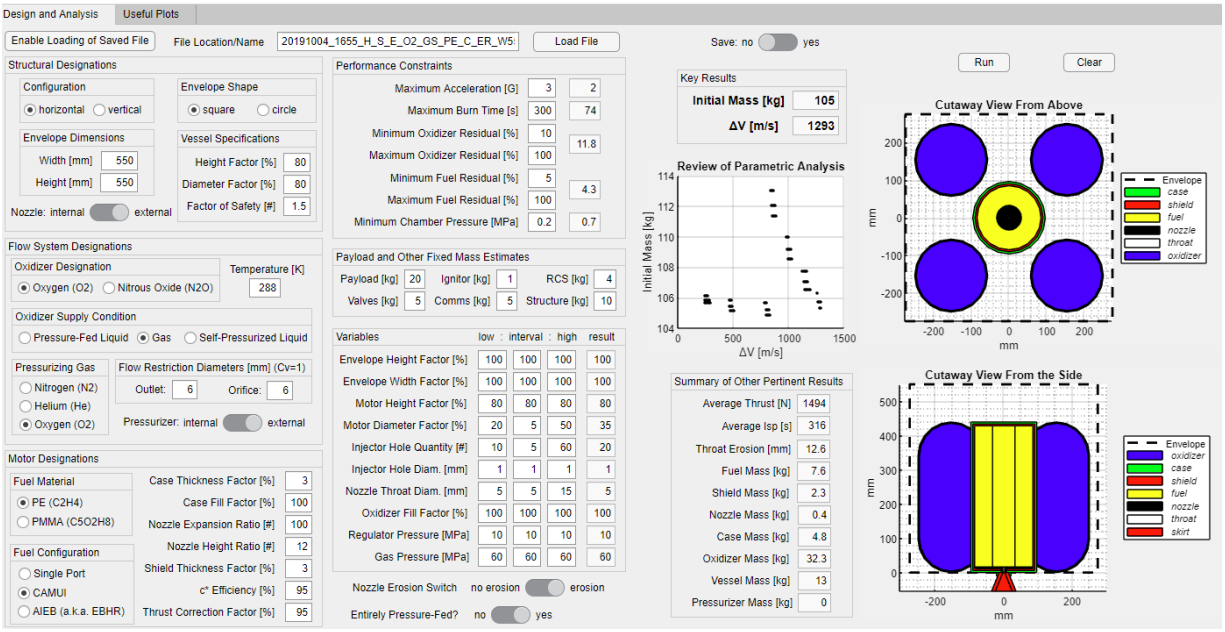

Screen Capture of SHARE_Designer

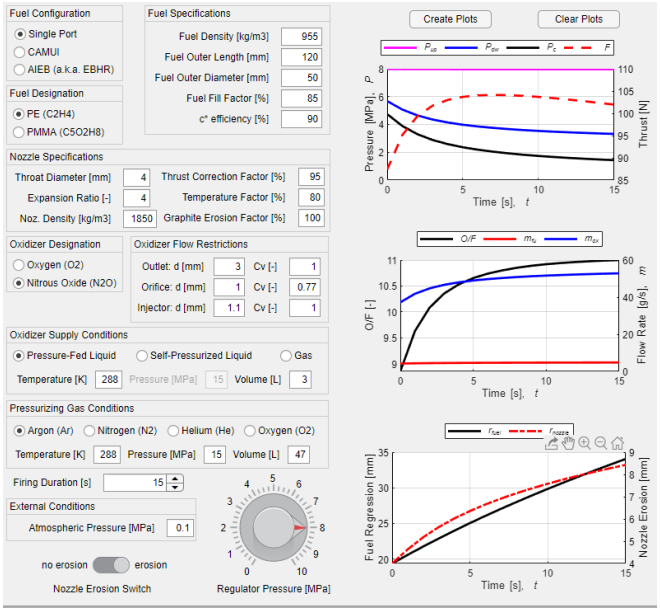

Screen Capture of Firing_Test_Simulator

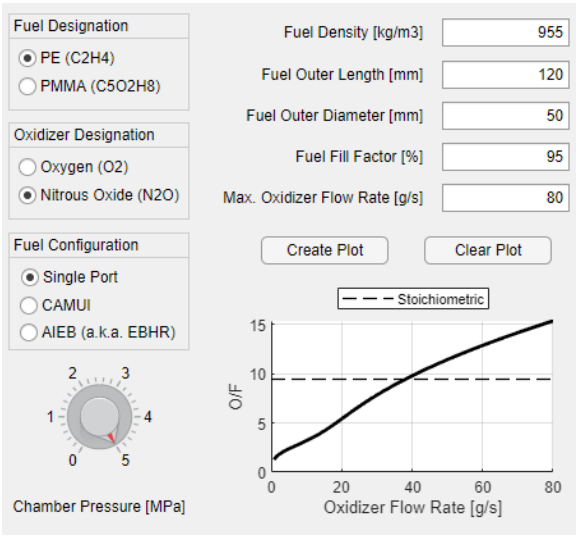

Screen Capture of Fuel_Designer

Appendix B (Schematics of Case A thru C)

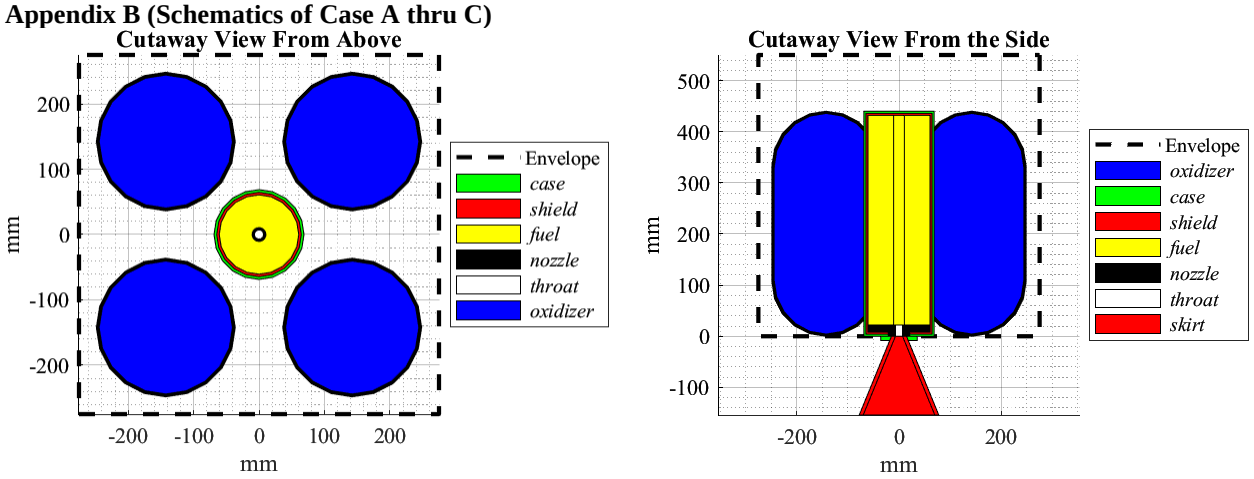

(a) Self-pressurized liquid N_2O/HDPE thruster: initial mass: 95 kg ΔV: 1412 m/s

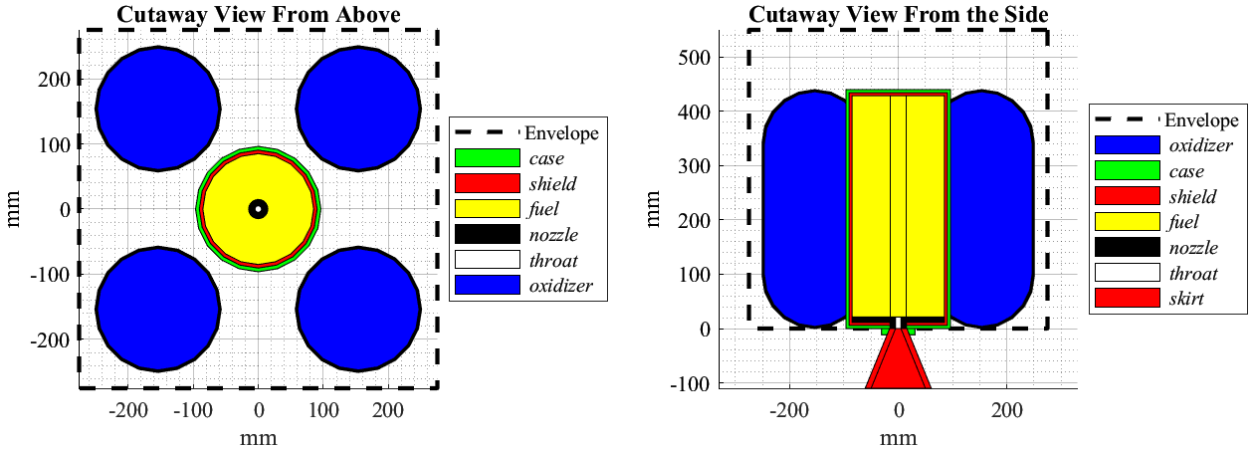

(b) Blowdown O_2/HDPE thruster: initial mass: 107 kg ΔV: 1326 m/s

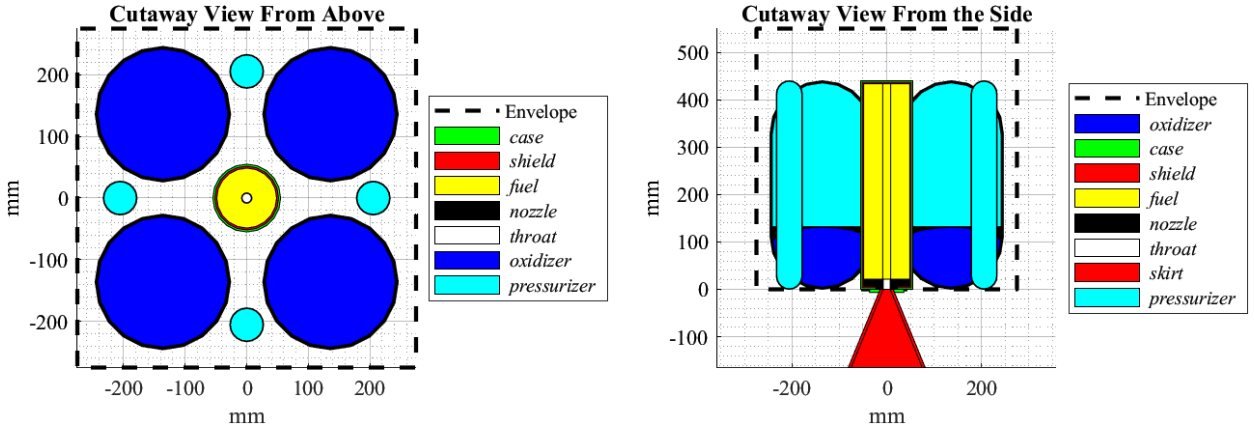

(c) Combination liquid N_2O-gas O_2/HDPE thruster: initial mass: 82 kg ΔV: 752 m/s